

# Novel Human Lung Tissue Model for the Study of SARS-CoV-2 Entry, Inflammation and New Therapeutics

Judith Grau-Expósito<sup>1\*</sup>, David Perea<sup>1\*</sup>, Marina Suppi<sup>1</sup>, Núria Massana<sup>1</sup>, Ander Vergara<sup>2</sup>, Maria José Soler<sup>2</sup>, Javier García-Pérez<sup>3</sup>, José Alcamí<sup>3,4</sup>, Anna Serrano-Mollar<sup>5,6</sup>, Joel Rosado<sup>7</sup>, Vicenç Falcó<sup>1</sup>, Meritxell Genescà<sup>1\*</sup>, and Maria J. Buzon<sup>1\*</sup>

<sup>1</sup>Infectious Diseases Department, Vall d'Hebron Research Institute (VHIR), Hospital Universitari Vall d'Hebron, Universitat Autònoma de Barcelona, Barcelona, Spain. VHIR Task Force COVID-19.

<sup>2</sup>Nephrology Research Department, Vall d'Hebron Research Institute (VHIR), Hospital Universitari Vall d'Hebron, Universitat Autònoma de Barcelona, Barcelona, Spain. VHIR Task Force COVID-19.

<sup>3</sup>AIDS Immunopathology Unit, National Center of Microbiology, Instituto de Salud Carlos III, Madrid, Spain.

<sup>4</sup>Clinic HIV Unit, Hospital Clinic, IDIBAPS, Barcelona, Spain.

<sup>5</sup>Experimental Pathology Department, Institut d'Investigacions Biomèdiques de Barcelona, Consejo Superior de Investigaciones Científicas (IIBB-CSIC), Institut d'Investigacions Biomèdiques August Pi i Sunyer (IDIBAPS), Barcelona, Spain.

<sup>6</sup>Centro de Investigaciones Biomédicas en Red de Enfermedades Respiratorias (CIBERES), Madrid, Spain.

<sup>7</sup>Thoracic Surgery and Lung Transplantation Department, Vall d'Hebron Institut de Recerca (VHIR), Hospital Universitari Vall d'Hebron, Barcelona, Spain. VHIR Task Force COVID-19.

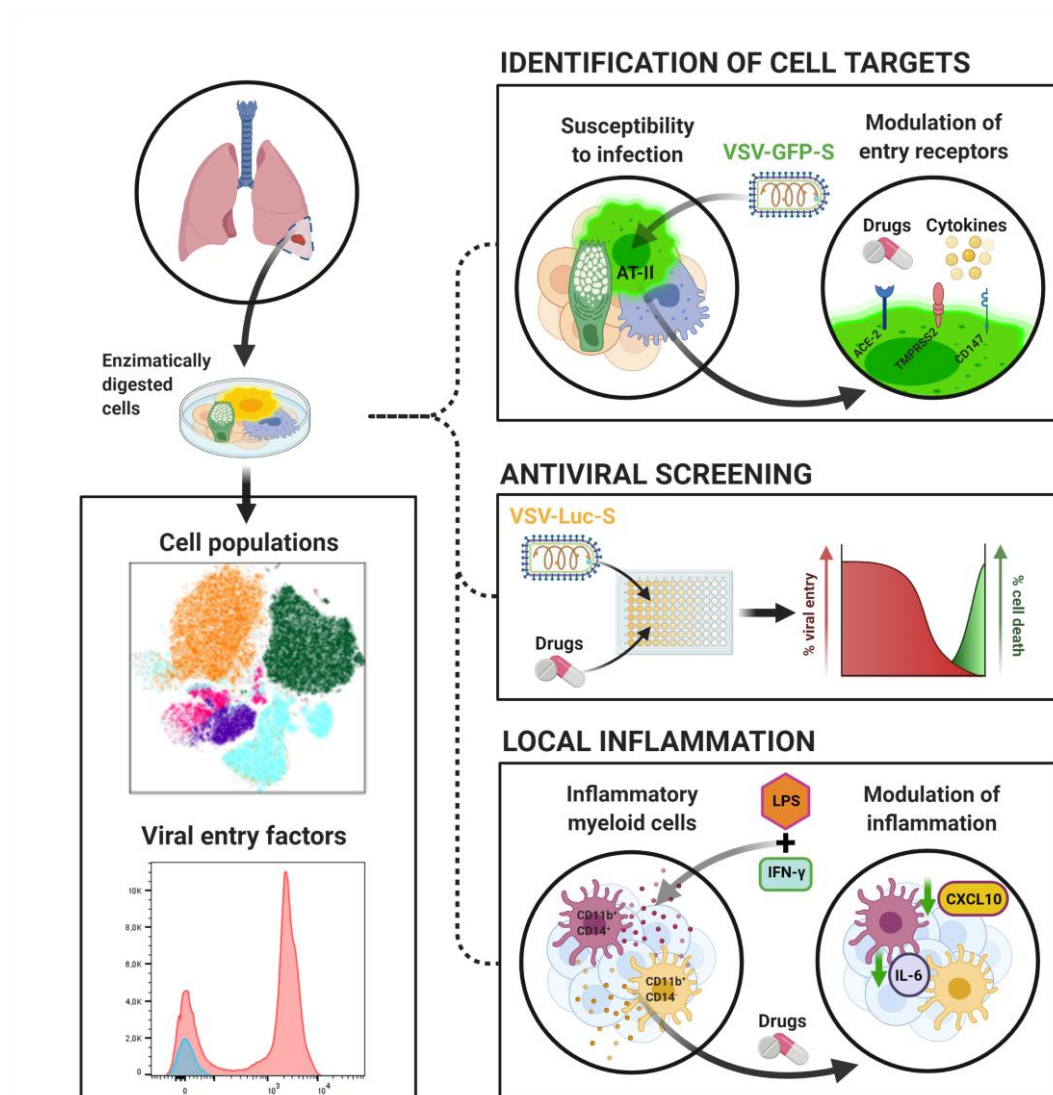
**Running title:** Human lung for the study of SARS-CoV-2

**Corresponding authors\*:** Maria J. Buzon ([mariajose.buzon@vhir.org](mailto:mariajose.buzon@vhir.org)) and Meritxell Genescà ([meritxell.genesca@vhir.org](mailto:meritxell.genesca@vhir.org))

## 26      **Abstract**

27      The development of physiological models that reproduce SARS-CoV-2 infection in primary  
 28      human cells will be instrumental to identify host-pathogen interactions and potential  
 29      therapeutics. Here, using cell suspensions from primary human lung tissues (HLT), we have  
 30      developed a platform for the identification of viral targets and the expression of viral entry  
 31      factors, as well as for the screening of viral entry inhibitors and anti-inflammatory compounds.  
 32      We show that the HLT model preserves its main cell populations, maintains the expression of  
 33      proteins required for SARS-CoV-2 infection, and identifies alveolar type II (AT-II) cells as the most  
 34      susceptible cell targets for SARS-CoV-2 in the human lung. Antiviral testing of 39 drug candidates  
 35      revealed a highly reproducible system, and provided the identification of new compounds  
 36      missed by conventional systems such as VeroE6. Using this model, we also show that interferons  
 37      do not modulate ACE2 expression, and that stimulation of local inflammatory responses can be  
 38      modulated by different compounds with antiviral activity. Overall, we present a novel and  
 39      relevant physiological model for the study of SARS-CoV-2.

# 40 Synopsis



41

42 *Ex vivo* physiological systems for the study of SARS-CoV-2-host interactions are scarce. Here, we  
 43 establish a novel model using primary human lung tissue (HLT) for the analysis of cell tropism  
 44 and identification of therapeutics.

- 45 • The HLT model preserves main cell subpopulations, including alveolar type-2 cells,  
 46 and expression of SARS-CoV-2 entry factors ACE2, CD147, and TMPRSS2.
- 47 • The HLT model is readily susceptible to SARS-CoV-2 entry.
- 48 • Antiviral testing in the HLT model allows the identification of new candidates missed  
 49 by conventional systems.
- 50 • Local inflammation is supported in the HLT model and offers the identification of  
 51 relevant anti-inflammatory compounds for SARS-CoV-2 infection.

## Introduction

We are facing a global health emergency, the COVID-19 pandemic, caused by the novel SARS-CoV-2 virus. There is currently no specific treatment to cure SARS-CoV-2 infection to limit disease progression of associated COVID-19. Early clinical trials showed promising drug candidates; remdesivir, a compound that inhibits the RNA synthesis of SARS-CoV-2, was superior to placebo in shortening the time to recovery in adults who were hospitalized with COVID-19 [1], however, the *Solidarity* trial failed to support this observation [2]. Recently, plitidepsin, a molecule that targets the eEF1A host protein has shown potent preclinical efficacy against SARS-CoV-2 [3]. Importantly, the development of *Acute Respiratory Distress Syndrome* in severe COVID-19 patients has been linked to dysregulated inflammatory responses. In this regard, the glucocorticoid dexamethasone decreased 28-day mortality among patients receiving invasive mechanical ventilation, but no benefit was observed in patients without respiratory support [4]. Thus, no effective treatment is currently available for COVID-19, and the rapid identification of antivirals with the potential to be easily transferred into the clinic could save human lives.

Screening of novel drug candidates is often performed using cell lines. In this sense, the most widely used cell lines for SARS-CoV-2 studies are epithelial cells derived either from lung (Calu-3), kidney (VeroE6), or colon (CaCo-2) [5]. These immortalized systems are highly reproducible and easy to handle but lack physiological relevance. The differential gene expression profiling of cell lines compared with primary cells from tissues might significantly affect important enzymes involved in the viral replication cycle. For instance, the level of ACE2 expression, the main receptor used by SARS-CoV-2 for viral entry, is shown to be different in several cell lines [6], while only a small fraction of alveolar type II (AT-II) cells, the main target for SARS-CoV-2 in the lung, express ACE2 [7, 8]. In addition, SARS-CoV-2 spike (S) glycoprotein, which is responsible for viral entry into target cells, can be activated by several host proteases, such as furin, transmembrane serine proteinase 2 (TMPRSS2) and cathepsin L, in a pH-dependent or independent manner [9, 10]. Whereas in some cell lines S protein is activated by endosomal pH-dependent protease cathepsin L, in airway epithelial cells viral entry depends on the pH-independent TMPRSS2 protease [10]. Thus, it is currently not well defined if SARS-CoV-2 may utilize multiple cell-type-specific host proteins for viral replication in primary target tissues and therefore, the potency of therapeutics directed against these proteins may also differ.

Further, inflammatory immune responses might also impact viral dynamics in the lung by affecting the expression of entry receptors. In this sense, early studies discovered that ACE2 was a human interferon-stimulated gene (ISG); IFN- $\beta$  and IFN- $\gamma$  were shown to strongly upregulate

the expression of ACE2 at the mRNA and cell surface protein levels, indicating that inflammatory molecules could shape cell susceptibility to viral infection [11]. However, how anti-inflammatory drugs may affect ACE2 expression and facilitate SARS-CoV-2 infection remains to be elucidated. One study reported that the use of nonsteroidal anti-inflammatory drugs (NSAIDs), such as ibuprofen, was linked to enhanced ACE2 expression in a diabetic-induced rat model [12] and other reports raised alarms regarding the possible role of NSAIDs at increasing susceptibility to SARS-CoV-2 infection [13, 14]. On the contrary, experimental and clinical evidence show that medium-to-low-dose glucocorticoids may play a protective role in COVID-19 by activating ACE2 and suppressing the associated cytokine storm [15]. Overall, the use of more relevant and physiological models for the study of either SARS-CoV-2 infection, the identification of drug candidates, or the impact of new therapeutics on the disease could significantly advance the successful translation of the results into the clinic.

Primary epithelial cell cultures of nasal and proximal airway epithelium have been used to study SARS-CoV-2 infection in the upper airways [8, 16-18]. Similarly, organ on-chip and organoids models of AT-II cells have been successfully developed [17, 19]. While very promising, these models still miss certain aspects of cellular complexity present in primary tissues [20]. In this regard, establishing a human lung tissue (HLT) model could offer a physiologically relevant alternative to *in vitro* and *in vivo* approaches for several reasons; it mimics the main site of viral replication in the lung, and contains all heterogeneous cell components present in the tissue with greater functional complexity compared to cell lines. Although still representing a reductionist *ex vivo* approach, it allows controlled experimental conditions. In the past, similar lung models have been successfully established to study the effect of allergens and inflammatory stimuli [21, 22]. Importantly, the HLT model allows mimicking an inflammatory local response that could be attenuated by anti-inflammatory drugs [23]. Furthermore, it has been used to provide low/medium throughput screening of anti-inflammatory candidate drugs for the treatment of airway diseases [23]. Significantly, lung tissues not only can be infected with SARS-CoV-2, but also generate local immune responses to viral infection [24]. Considering all these factors, here we aimed to develop and characterize a physiological and reproducible human lung tissue model, which could be used for the study of virus-host interactions, identification of potential antiviral compounds, as well as help investigating the role of inflammation in relation to SARS-CoV-2 infection.

# Results

## Characterization of the HLT model

To establish the HLT model, non-neoplastic areas from lung tissue resections were obtained from hospitalized non-COVID19 patients undergoing thoracic surgery. First, we optimized cell culture and digestion conditions, since the methodology used for tissue processing can significantly impact viability and function of target cell populations. Thus, we tested the preservation of AT-II, defined mainly by EpCAM and HLA-DR expression [25], and of several hematopoietic cell subsets, after tissue digestion with different enzymes. Flow cytometry gating strategy and cell markers used for identification of main populations are shown in **Figure S1A**. We observed that collagenase outperformed liberase and trypsin at preserving AT-II cells, the main SARS-CoV-2 target (**Figure S2A-B**). Among the hematopoietic cells present in the lung tissue we identified CD3 T (which represented  $1.94\% \pm 0.59$  out of the total live cell fraction), myeloid dendritic cells ( $0.03\% \pm 0.007$ ), monocytes/macrophages subsets ( $0.42 \pm 0.14\%$ ), neutrophils ( $1.80\% \pm 0.53$ ) and alveolar macrophages ( $0.05\% \pm 0.01$ ). Moreover, non-hematopoietic cells such as AT-II and endothelial cells represented  $0.24\% \pm 0.05$  and  $0.5\% \pm 0.15$  out of the total live cell fraction, respectively (**Figure 1A**). All populations have been previously identified in human lungs [24, 26, 27]. Moreover, the nature of AT-II cells in lung cell suspensions was confirmed by staining with phosphatase alkaline (**Figure 1B**), which has been shown to be a reliable marker of type II cell phenotype both *in vitro* and *in vivo* [28]. Next, we focus on the expression of previously identified proteins involved in viral entry. Single-cell transcriptome studies have shown that ACE2, one of the main host cell surface receptors for SARS-CoV-2 attachment and infection, is predominantly expressed by AT-II cells [8, 29]. Moreover, ACE2 expression wanes in distal bronchiolar and alveolar regions paralleled by SARS-CoV-2 infectivity [8]. In human parenchyma lung cells, we found ACE2 expression mainly in AT-II cells (**Figure 1C**), a finding that was confirmed by immunohistochemistry (**Figure 1D**). Percentage of AT-II cells expressing ACE2 was rather small and varied between individuals ( $6.29\% \pm 1.00$ ) (**Figure 1C**), as previously described [7]. We also studied the expression of CD147 on lung cells, which has been reported as a novel route of SARS-CoV-2 infection *in vitro* and *in vivo* models [30]. CD147 was ubiquitously expressed in several hematopoietic and non-hematopoietic cells (**Figure 1C**). Importantly,  $92.3\% \pm 1.14$  of AT-II cells expressed CD147 (**Figure 1C**). Similarly, and in agreement with other studies [31], TMPRSS2 protease expression was identified in AT-II cells ( $21.33\% \pm 7.52$ ) (**Figure 1C**). Overall, we found that human lung suspensions preserved critical cell populations and the expression of factors required for SARS-CoV-2 infection.

## Susceptibility of HLT cells to SARS-CoV-2 viral entry

Next, we assessed if HLT cells were susceptible to viral infection. We generated pseudotyped vesicular stomatitis virus (VSV) viral particles bearing the S protein of SARS-CoV-2 and expressing either luciferase (VSV\*ΔG (Luc)-S) or GFP (VSV\*ΔG (GFP)-S) reporter genes upon cell entry. As a control, we used the VSV-G virus, which has very broad cell tropism. As expected, VeroE6 cells were highly susceptible to SARS-CoV-2 entry, as demonstrated for VSV\*ΔG (GFP)-S and VSV-ΔG (Luc)-S (**Figure 2A**). Anti-ACE2 antibody blocked more than 90% of VSV\*ΔG (Luc)-S, but was inactive for VSV-G (Luc) infection (**Figure 2B**). This observation has been widely reported before [10, 32, 33], and identifies ACE2 as the main cell receptor required for viral entry in VeroE6. Importantly for viral pathogenesis, it has been postulated that SARS-CoV-2 S protein might downregulate ACE2 expression, as previously observed for SARS-CoV [34]. We consistently observed a significant strong reduction in ACE2 expression after viral entry (**Figure 2C**).

We then evaluated the susceptibility of HLT cells to viral entry, using the same viral constructs. HLT cells were readily infected with pseudotyped S particles (VSV\*ΔG (Luc)-S and VSV\*ΔG (GFP)-S), with the natural donor variation representative of primary samples (**Figure 2D**). As expected [8], lung cells compatible with an AT-II phenotype were identified as the main cell targets in steady conditions (**Figure 2E**). Blockade of ACE2 resulted in a donor-dependent reduction of viral infectivity, ranging from 50 to 100% (**Figure 2F**). Camostat, a TMPRSS2 inhibitor, significantly inhibited viral entry in all HLT assays, although the entry process was not always completely abrogated (**Figure 2F**), suggesting that AT-II cells may become infected through the use of alternative factors [35]. Similarly, the presence of an anti-CD147 antibody inhibited SARS-CoV-2 entry in AT-II cells (**Figure 2F**). Collectively, these data indicate that HLT cells are highly susceptible to SARS-CoV-2 viral entry, and that ACE2, CD147 and TMPRSS2 are important proteins for viral entry in human lung cells. Overall, these results support the value of the HLT model to successfully study SARS-CoV-2 viral entry, and related mechanisms, in a more physiological system.

## Antiviral assays in the HLT model

To validate the HLT model as a platform for the screening of antiviral candidates, we assayed potential antiviral compounds, most of them previously identified by computational methods with predicted ability to inhibit SARS-CoV-2 cell entry due to their interaction with S protein or with the interface S-ACE2 [36]. A detailed description of the 39 selected drugs is available in **Table S1**. HLT cells were exposed to VSV\*ΔG (Luc)-S virus in the presence of 1/5 serial dilution of the different tested compounds. 20h post-exposure, antiviral activity and cell viability were



measured by luminescence. Results in HLT cells were systematically compared with antiviral testing performed in the cell line VeroE6. Among 39 drugs that were evaluated in our study, 16 (41%) showed some antiviral activity against SARS-CoV-2 with  $EC_{50}$  values ranging from 0.5  $\mu$ M to 66  $\mu$ M (**Table S2**). We observed that 23% of drugs had concordant results between both models (**Figure 3**). Cepharanthine, a naturally occurring alkaloid reported to have potent anti-inflammatory and antiviral properties, was one of the most potent antivirals identified in both systems, with  $EC_{50}$  of 0.4  $\mu$ M and 6.1  $\mu$ M in VeroE6 and HLT cells, respectively (**Figure 3A and B**). Of note, we observed cell toxicity at the highest concentrations ( $CC_{50}$  VeroE6 = 22.3  $\mu$ M;  $CC_{50}$  HLT = 13.8  $\mu$ M), which translated in a satisfactory *selectivity index* (SI) in VeroE6 cells, but close to the standard threshold of 2 in HLT cells ( $SI_{VeroE6}$  = 55.7;  $SI_{HLT}$  = 2.2) [37]. The anti-SARS-CoV-2 activity of hydroxychloroquine, a compound known to interfere with endosomal acidification necessary for the proteolytic activity of cathepsins, has been extensively reported [38, 39]. In our study, we observed that hydroxychloroquine was equally effective at inhibiting viral entry in VeroE6 and HLT cells ( $EC_{50}$  VeroE6 = 1.58  $\mu$ M;  $EC_{50}$  HLT = 9.26  $\mu$ M) (**Figure 3A, B**), with no apparent cytotoxicity (**Figure 3C**). Ergoloid, an approved drug used for dementia, and recently identified as a potential inhibitor of SARS-CoV-2 main protease [40], induced a ~90% viral entry inhibition in HLT cells at non-toxic concentrations (**Figure 3A-C**). Indeed, *SI* for this compound was higher in the HLT model than in VeroE6 cells ( $SI_{VeroE6}$  = 3.9;  $SI_{HLT}$  = 11.38). Similarly, ivermectin, a broad-spectrum anti-parasitic compound, showed very similar antiviral potency in both models, however *SI* greatly differed ( $SI_{VeroE6}$  = 1.4;  $SI_{HLT}$  = 8). Additionally, we also calculated the *Coefficient of Variation* (CV) of the antiviral assays as a measure of relative variation in 50% Effective Concentration ( $EC_{50}$ ) values. We show that the CV varied from 0.9 to 15.36% in HLT cells (**Figure 3D**). The low CV obtained highlights the suitability of the HLT model for the identification of antivirals.

We also detected discordant antiviral results between both models (**Figure 4**). Indeed, 5 drugs inhibited SARS-CoV-2 entry in HLT cells without affecting cell viability, but no effect was observed in VeroE6 (**Figure 4A-C**). As expected, camostat, a TMPRSS2 inhibitor [41], was not active in VeroE6 cells due to lack of TMPRSS2 expression in this cell line. However, camostat was highly active in HLT cells ( $EC_{50}$  = 2.7  $\mu$ M). Indeed, a clinical trial testing its potential to prevent SARS-CoV-2 transmission is ongoing (NCT04625114). Further, sulindac, a nonsteroidal anti-inflammatory drug, and valaciclovir, an antiviral drug, presented some inhibitory potential at 100  $\mu$ M only in HLT cells. Interestingly, phenformin, an antidiabetic drug and an mTOR inhibitor, has been postulated as an inhaled drug candidate against influenza and coronavirus infections [42]. Phenformin reduced the incidence of influenza infection in diabetic patients during the



1971 outbreak [42]. Here, we observed that phenformin significantly reduced viral entry starting at 4 $\mu$ M only in HLT cells, supporting previous recommendations as inhaled treatment. Finally, eriodictyol, a flavonoid used as a medicinal plant [43], demonstrated certain activity at 20-100 $\mu$ M. In contrast, luteolin induced potent viral entry suppression only in VeroE6 cells at high concentrations (**Figure 4A-C**). Overall, these results indicate that the HLT is a reproducible and highly relevant model for antiviral testing in a physiological system that recapitulates main antiviral activities observed in cell models, and offers the identification of new compounds missed by conventional systems.

## **Impact of inflammation and anti-inflammatory drugs on ACE2 expression and SARS-CoV-2 viral entry**

Since SARS-CoV-2 viral infection rapidly induces an inflammatory response, we wondered if certain components of this response could modulate ACE2 expression, potentially allowing increased viral binding of SARS-CoV-2 and thus, enhancing infection. Further, ACE2 has been previously identified as an ISG or a component of the IFN-signaling pathway [11, 44], and a recent investigation showed that cultured human primary basal epithelial cells treated with IFN- $\alpha$ 2 and IFN- $\gamma$  led to upregulation of ACE2 [11]. Moreover, IL-1 $\beta$  and IFN- $\beta$  upregulated ACE2 in large airway epithelial cell cultures [8]. Thus, considering that type I interferons represent a first line of defence against viral infections and that several cytokines are rapidly induced and associated with disease severity in COVID-19 patients [45], we tested the effects of different molecules on ACE2 expression in our model. In initial experiments, we tested three different doses of a wider range of molecules (including tumor necrosis factor (TNF), IL-6 and IFN- $\gamma$ ), which were used to select doses and compounds of interest. Finally, the effect of IFN- $\alpha$ 2, IFN- $\beta$ 1, IL-1 $\beta$ , IL-10 and GM-CSF on ACE2 expression was evaluated in the HLT model. Cells were then treated with selected immune stimuli and cultured for 20h, when the expression of ACE2 in AT-II cells was evaluated by flow cytometry. The only significant change we observed was for IL-1 $\beta$  stimulation, which decreased the fraction of AT-II cells expressing ACE2 (**Figure 5A**). No other significant changes were observed. Overall, we show that relevant inflammatory stimuli have a limited impact on ACE2 expression in AT-II cells, while the effect and impact of IL-1  $\beta$  on viral infection should be further explored.

It is currently not well documented if anti-inflammatory drugs could modulate ACE2 expression, and consequently, might impact susceptibility to SARS-CoV-2 infection [46]. Several glucocorticoids have shown to impart activating effects on ACE2 expression in cell lines; cortisol showed the strongest effect on ACE2 activation, followed by prednisolone, dexamethasone, and

249 methylprednisolone [15]. Moreover, NSAIDs, compounds that inhibit cyclooxygenase-1 and 2  
250 mediating the production of prostaglandins, which play a role in inflammatory responses, have  
251 been linked to ACE2 upregulation [15]. Here, we took advantage of our HLT model to study the  
252 effect of several anti-inflammatory drugs on both ACE2 expression and SARS-CoV-2 viral entry.  
253 1/5 dilutions of ibuprofen, cortisol, dexamethasone and prednisone were added to HLT cells for  
254 20h. Overall, no effect on ACE2 expression was observed after the addition of these anti-  
255 inflammatory drugs (**Figure 5B**). Consequently, the antiviral assay showed no major impact of  
256 anti-inflammatory compounds on viral entry; however, high concentrations of prednisone and  
257 dexamethasone showed a partial reduction of viral entry in HLT cells, without any apparent  
258 impact on VeroE6 (**Figure 5C**). Thus, we show that selected anti-inflammatory drugs have limited  
259 impact on ACE2 expression within AT-II cells present in the HLT model, as well as in SARS-CoV-2  
260 viral entry.

### 261 **Anti-inflammatory properties of selected compounds**

262 Last, we were interested in modelling the anti-inflammatory properties of several drugs in  
263 our HLT model. Based on their antiviral potency in HLT cells, we selected cepharanthine,  
264 ergoloid, camostat, ivermectin, hydroxychloroquine and ciclesonide for further evaluation. Of  
265 note, some of these drugs have been previously identified as immunomodulators with anti-  
266 inflammatory effects (**Table S1**). However, their direct impact on inflammatory molecules  
267 directly secreted by human lung cells has not been evaluated. HLT cells were stimulated with  
268 lipopolysaccharides (LPS) and IFN- $\gamma$  in the presence of these antivirals and, 20h after, the  
269 expression of IL-6 and CXCL10, a potent pro-inflammatory cytokine and chemokine respectively,  
270 was intracellularly measured by flow cytometry. As shown in **Figure 6A**, two major  
271 subpopulations of myeloid cells contributed to the upregulation of CXCL10 and IL-6 expression  
272 upon stimulation. Myeloid CD11b<sup>+</sup>CD14<sup>+</sup> were the cells with a greater response, showing 50%  
273 of cells expressing IL-6 and 30% expressing CXCL10 after stimulation (**Figure 6B**). Using this  
274 model of local inflammation, we tested the capacity of the selected compounds to modify this  
275 response. We observed that camostat had the most potent effect, which significantly reduced  
276 the expression of CXCL10 in CD11b<sup>+</sup>CD14<sup>+</sup> and of IL-6 in CD11b<sup>+</sup>CD14<sup>+</sup> myeloid subsets (**Figure**  
277 **6B**). Ergoloid, which has not been linked to modulation of inflammation before, significantly  
278 reduced the expression of cytokines in CD11b<sup>+</sup> CD14<sup>+</sup> myeloid cells, and cepharantine reduced  
279 IL-6 production from this subset. Finally, ciclesonide induced CXCL10 secretion in CD11b<sup>+</sup>CD14<sup>+</sup>  
280 myeloid cells (**Figure 6B**). Altogether, our results validate the HLT model as a relevant method  
281 for the identification of anti-inflammatory compounds impacting specific pro-inflammatory cell  
282 populations from the lung parenchyma.

## Discussion

The emergency created by the rapid spread of SARS-CoV-2 infection worldwide required a quick response from physicians treating these patients, who adapted to the rapid knowledge being generated by both clinical practice and basic research. However, up to date, no specific drugs against SARS-CoV-2 have been approved for clinical use. In this sense, the choice of the cell and animal models used to test the efficacy of antivirals will impact its rapid translation into the clinics. Here, we have developed a novel human lung tissue (HLT) model that can be safely performed in a BSL2 facility, which allows i) the identification of cell targets and expression of viral entry factors, ii) the impact of inflammation on host-pathogen interactions and iii) a rapid medium-high throughput drug screening of SARS-CoV-2 entry inhibitors and local anti-inflammatory candidates.

While cell lines have been traditionally used for the screening of potential antiviral compounds due to their reproducibility, as well as being quick and user-friendly assays, they lack physiological relevance. Similarly, entry receptors and viral factors have been identified using immortalized cell lines [10, 47], and cell targets for SARS-CoV-2 in tissues have been mainly determined by analyzing the expression of viral entry factors in RNA-seq datasets [48] or using replication-competent SARS-CoV-2 isolates in BSL3 facilities [49]. Importantly, these studies have identified AT-II cells as main viral targets for SARS-CoV-2 infection in the lungs, and the molecules ACE2, CD147 and TMPRSS2 as the main factors for viral entry [10, 30, 50]. However, the development of more refined and translational *ex vivo* models of SARS-CoV-2 entry will not only have implications for understanding viral pathogenesis, but also will be useful for the characterization of cell targets under specific conditions and the identification of potential antivirals blocking infection of primary cells. In our HLT model, the maintenance of cell type complexity in their *in vivo* proportions may represent a significant advantage over previous models [17, 19, 51]. Using pseudotyped viral particles expressing SARS-CoV-2 spike, we first corroborated that AT-II cells are the primary cell target in lung tissue in steady conditions. This agrees with several studies using different approximations [11, 52, 53] and validates our primary model for viral tropism identification.

Moreover, we showed that the HLT model can be successfully used for drug screening purposes. We tested 39 drugs and compared the results with antiviral testing in VeroE6 cells. Not surprisingly, we showed discordant results between both models. Indeed, we found that 37.5% of the tested compounds had discordant results between HLT and VeroE6 cells; 31.25% of drugs showed some antiviral effect in HLT but no activity was detected in VeroE6, and 6.2%

showed only antiviral effects in VeroE6 cells. Among other reasons, the differential expression of several key proteins needed for viral entry, might explain current discrepancies between models. Importantly, using the HLT model, we identified several compounds with antiviral activity; cepharanthine showed an  $EC_{50}$  of 6.1 $\mu$ M and concordantly, it was recently identified in a high throughput screening as one of the most potent drugs against SARS-CoV-2 [54], likewise several other studies have pointed towards this drug as a potent entry and post-entry SARS-CoV-2 inhibitor [55]. Instead, for hydroxychloroquine, an early report suggested no antiviral activity in human lung cells due to different expression of the required proteases for viral entry [56]. In our study, however, we observed that this drug was equally effective at inhibiting viral entry in VeroE6 and HLT cells. Nevertheless, clinical trials failed to show effectiveness of this drug as a treatment for COVID-19 [57-59]. Recently, a strong dependency of SARS-CoV-2 on TMPRSS2 for viral entry, rather than on cathepsin L, was identified as a possible mechanistic explanation for its failure *in vivo* [60]. Similarly, we identified ivermectin as an effective antiviral in HLT cells. Of note, ivermectin received limited attention as a potential drug to be repurposed against COVID-19 based on its limited ability to reach lung tissue *in vivo* [61]. Further, a clinical trial failed to show a reduction in the proportion of PCR-positive patients seven days after ivermectin treatment [62].

Importantly, the HLT model also provides a platform for testing anti-inflammatory drugs and the modulation of viral entry factors with drug candidates and immunomodulatory stimuli. We showed that IL-1 $\beta$  was able to reduce ACE2 expression in AT-II cells, in contrast to other cytokines induced during SARS-CoV-2 infection like IFN- $\alpha$ 2, IFN- $\beta$ 1, IL-10 and GM-CSF, which did not impact ACE2 protein production. In primary epithelial cells derived from healthy nasal mucosa, Ziegler et al. [11] showed a significant induction of ACE2 transcripts after IFN- $\alpha$ 2 and IFN- $\gamma$  stimulation, as well as and in a human bronchial cell line treated with either type I or type II IFN. Moreover, the authors showed that influenza A virus infection increased ACE2 expression in lung resections [11], strongly suggesting that ACE2 was an ISG. However, following studies showed that ACE2 transcription and protein production was not responsive to IFN. Instead, they described a new RNA isoform, MIRb-ACE2, that was highly responsive to IFN stimulation, but importantly, encoded a truncated and unstable protein product [63, 64]. These results highlight the need to validate scRNA-seq data with orthogonal approaches, such as the confirmation of protein expression levels in relevant systems. In the HLT model, we quantified ACE2 protein expression and importantly, focused our analysis on AT-II cells, the main SARS-CoV-2 targets in lung parenchyma. Also, in agreement with our results, a primary human bronchial epithelial cell model, type I ( $\beta$ ), II ( $\gamma$ ), or III ( $\lambda$ 1) IFNs did not induced ACE2 expression [65]. Moreover, a study

performed by Lang et al [66], showed that IFN- $\gamma$  and IL-4 downregulate the SARS-CoV receptor ACE2 in VeroE6 cells, and similarly, stimulation of A549 cells with IFN- $\alpha$ , IFN- $\gamma$ , and IFN- $\alpha$ +IFN- $\gamma$  did not identify ACE2 as an ISG [67].

A feasible explanation for the increase of ACE2 protein production upon IL-1  $\beta$  treatment is that IL-1 $\beta$  activates disintegrin and metalloproteinase domain-containing protein 17 (ADAM17) [68], which mediates the shedding of ACE2 [69]. Although this effect would seem positive to reduce SARS-CoV-2 infection, ACE2 is a lung-protective factor, as it converts Angiotensin (Ang) II to Ang-(1–7); while Ang II promotes harmful effects in the lung, e. g. fibrosis, vasoconstriction, inflammation, endothelial dysfunction, edema, and neutrophil accumulation[70], Ang-(1-7) has counter-regulatory effects protective of lung injury. Moreover, Ang-(1–7) plays an essential role in hemostasis, as it favors anti-thrombotic activity in platelets [71]. In any case, treatment of COVID-19 patients with respiratory insufficiency and hyper inflammation with IL-1 inhibitors was associated with a significant reduction of mortality [72], indicating that at least during severe COVID-19 the overall effect of IL-1 $\beta$  is detrimental. While the reduction of ACE2 expression in AT-II cells by IL-1 $\beta$  may be of interest, it needs to be determined if in combination with other cytokines rapidly induced during viral respiratory infection [73], this effect would remain.

Further, glucocorticoids and NSAIDS have been linked to ACE2 upregulation previously [15]. In contrast, we did not observe any significant impact of ibuprofen, cortisol, dexamethasone and prednisone on ACE2 protein expression. These results are concordant with a recent report showing that suppression of cyclooxygenase (COX)-2 by two commonly used NSAIDs, ibuprofen and meloxicam, had no effect on ACE2 expression, viral entry, or viral replication in a mouse model of SARS-CoV-2 infection [74]. Moreover, dexamethasone incompletely reduced viral entry. This observation partially agrees with a study using lung cells previously treated with dexamethasone, which showed significant suppression of SARS-CoV-2 viral growth [24].

In addition, we used the model for testing local inflammation and potential anti-inflammatory drugs. Several resident and recruited myeloid subsets may contribute to the rapid cytokine storm detected in COVID-19 patients [75-77]. Thus, the identification of antiviral drugs that can also limit the extent of these initial pro-inflammatory events may offer added value to the overall therapeutic effect of a given drug. In this sense, we observed that camostat significantly reduced the expression of proinflammatory molecules IL-6 and CXCL10 in several myeloid CD11b<sup>+</sup> subsets. Concordantly, in a previous study using primary cultures of human tracheal epithelial cells infected with H1N1 virus, camostat also reduced the concentrations of the cytokines IL-6 and TNF in cell supernatants [78], suggesting a potent anti-inflammatory

potential. In contrast, ivermectin did not affect the expression of cytokines in our model. Differing from previous results, ivermectin was shown to have anti-inflammatory effects in mice and *in vitro* using murine macrophages; ivermectin reduced the production of TNF, IL-1 and IL-6, and suppressed LPS-induced NF- $\kappa$ B translocation[79]. Of note, our HLT model of inflammation is optimized up to detect changes in the intracellular expression of cytokines by local myeloid cells, and thus, how these intracellular changes reflect total cytokine production in supernatant needs further evaluation.

Finally, it is also important to note the potential limitations of the model, including the limited availability of human lung samples, inter-patient variation (age, smoking, etc.), the effects on lung biology of the medical condition instigating surgery, and the location of the sample resection which may affect the proportion of cell subsets such as AT-II. However, this variability is what shapes the HLT into a highly physiological and relevant model in comparison to current methods based on immortalized cell cultures. Besides the interest of the model proposed here, our results highlight drugs with antiviral activity in HLT cells together with immunomodulatory properties, which could increase the benefit of this treatment during COVID-19 disease progression. For instance, camostat, cepharantine and ergoloid were three of the most potent drugs inhibiting SARS-CoV-2 entry, and remarkably, also exerted a significant anti-inflammatory effect on myeloid cells. Clinical trials with camostat, currently ongoing, ergoloid and cepharantine, will shed light on their use as both antivirals and anti-inflammatory compounds.

## Materials and methods

### Cells and virus

VeroE6, isolated from kidney epithelial cells of an African green monkey, were grown in DMEM medium supplemented with 10% fetal bovine serum (FBS; Gibco) 100 U/ml penicillin, and 100 µg/ml streptomycin (Capricorn Scientific) (D10) and maintained at 37°C in a 5% CO<sub>2</sub> incubator.

The spike of the SARS-CoV-2 virus was generated (GeneArt Gene Synthesis, ThermoFisher Scientific) from the codon-optimized sequence obtained by Ou et al.[35] and inserted into pcDNA3.1D/V5-His-TOPO (pcDNA3.1-S-CoV2Δ19-G614). This plasmid presents the mutation D614G and a deletion in the last 19 amino acids from the original spike. Pseudotyped viral stocks of VSV\*ΔG(Luc)-S were generated following the protocol described by Whitt [80] with some modifications. Briefly, 293T cells were transfected with 3µg of the plasmid encoding the SARS-CoV-2 spike. Next day, cells were infected with a VSV-G-Luc virus (MOI=1) (generated from a lentiviral backbone plasmid that uses a VSV promoter to express luciferase) for 2h and gently washed with PBS. Cells were incubated overnight in D10 supplemented with 10% of I1 hybridoma (anti-VSV-G) supernatant (ATCC CRL-2700) to neutralize contaminating VSV\*ΔG(Luc)-G particles. Next day, the resulting viral particles were collected and titrated in VeroE6 cells by enzyme luminescence assay (Britelite plus kit; PerkinElmer), as described previously [81].

### Lung tissue

Lung tissues were obtained from patients without previous COVID-19 history and a recent negative PCR test for SARS-CoV-2 infection undergoing thoracic surgical resection at the Thoracic Surgery Service of the Vall d'Hebron University Hospital. Study protocol was approved by the Ethical Committee (Institutional Review Board number PR(AG)212/2020). Non-neoplastic tissue areas were collected in antibiotic-containing RPMI 1640 and immediately dissected into approximately 8-mm<sup>3</sup> blocks. These blocks were first enzymatically digested with 5 mg/ml collagenase IV (Gibco) and 100 µg/ml of DNase I (Roche) for 30 min at 37°C and 400 rpm and, then, mechanically digested with a pestle. The resulting cellular suspension was filtered through a 70µm-pore size cell strainer (Labclinics) and washed twice with PBS. Pellet recovered after centrifugation was resuspended in fresh medium (RPMI 1640 supplemented with 5% FBS, 100 U/ml penicillin, and 100 µg/ml streptomycin) and DNase I to dissolve cell aggregates, and the resulting cell suspension was then filtered through a 40µm-pore size cell strainer (Labclinics).



Cell number and viability were assessed with LUNA™ Automated Cell Counter (Logos Biosystems). For cell phenotyping the following antibodies were used: anti-CD31 (PerCP-Cy5.5, BioLegend), anti-CD11b (FITC, BioLegend), anti-CD11c (Pe-Cy7, BD Biosciences), anti-E-cadherin (Pe-CF594, BD Biosciences), primary goat anti-ACE2 (R&D systems), anti-CD14 (APC-H7, BD Biosciences), anti-CD45 (AF700, BioLegend), anti-EpCAM (APC, BioLegend), anti-CD3 (BV650, BD Biosciences), anti-CD15 (BV605, BD Biosciences) and anti-HLA-DR (BV421, BioLegend). For ACE2 detection, after surface staining, cells were stained with secondary donkey anti-goat IgG (PE, R&D Systems) for 30 min at 4 °C. Cell viability was determined using an AQUA viability dye for flow cytometry (LIVE/DEAD fixable AQUA, Invitrogen). In some experiments, instead of CD11b or CD15, we used a primary rabbit anti-TMPRSS2 or anti-CD147 (BV605, BD Biosciences), respectively. For TMPRSS2 detection, after ACE2 staining with the appropriate secondary antibody, cells were washed twice with PBS 1% NMS (normal mouse serum) and then stained with a secondary goat anti-rabbit IgG (AF488, ThermoFisher) for 30 min at 4°C. After fixation with PBS 2% PFA, cells were acquired in an LSR Fortessa (BD Biosciences), and data were analyzed using the FlowJo v10.6.1 software (TreeStar).

#### **Cytospin and alkaline phosphatase staining**

Cytospin preparations were obtained from freshly isolated human lung cells at an approximate density of 150,000 cells/slide, and air-dried during 15 min. Cells were stained with alkaline phosphatase, as an enzyme marking epithelial type II cells, following manufacturer's instructions (Alkaline phosphatase Kit, Sigma). The intensity of pink stain reflects the amount of alkaline phosphatase in positive cells.

#### **ACE2 immunohistochemical staining in human lung tissue sections**

Human lungs were maintained in 10% formalin for 24 hours and then embedded in paraffin. Paraffin-embedded lungs were cut into 4 µm sections. After removing the paraffin, endogenous peroxidases were inactivated in an aqueous solution containing 3% H<sub>2</sub>O<sub>2</sub> and 10% methanol and antigen retrieval was performed heating the samples in citrate buffer (10mM citric acid, pH 6.0). The sections were then blocked in bovine serum albumin (5%), incubated with anti-ACE2 antibody (R&D Systems cat. n° AF933, dilution 1:100) and with biotinylated secondary antibody against goat IgGs (Vector Laboratories cat. n° BA-9500, dilution 1:250). Proteins were visualized using the ABC Peroxidase Standard Staining Kit (ThermoFisher) followed by 3,3'-Diaminobenzidine (DAB) Enhanced Liquid Substrate System (Sigma Aldrich). Counterstaining was done with hematoxylin.

## Antiviral screening assay

The complete list of compounds tested in this study, including information about its clinical use, product reference and vendors is shown in **Table S1**. Duplicates of five-fold serial dilutions of 39 antiviral compounds were tested in both VeroE6 cell line and in human lung tissue (HLT) cells using at least 2 different donors. For VeroE6, five-fold serial dilutions of the compounds, ranging from 100µM to 0,25nM, were prepared in D10 in a 96-well flat-bottom plates. VeroE6 cells were added at a density of 30.000 cells/well and incubated with the drug for at least 1 h before infection. Subsequently, cells were infected with 1,500 TCID<sub>50</sub> of VSV\*ΔG(Luc)-S virus. In parallel, drug cytotoxicity was monitored by luminescence. To evaluate the antiviral activity of drugs in HLT cells, five-fold serial dilutions of the compounds, ranging from 100µM to 0.8µM or 6.4nM, were prepared in R10 in a 96-well conic bottom plates. HLT cells were added at a density of 300,000 cells/well and incubated with the compound for at least 1h before infection. Then, MOI 0,1 of VSV\*ΔG(Luc)-S virus were added to wells, and plates were spinoculated at 1,200g and 37°C for 2h. After infection, fresh medium was added to the wells and cell suspensions were transferred into a 96-well round-bottom plate. Cells were then cultured overnight at 37°C in a 5% CO<sub>2</sub> incubator. Each plate contained the following controls: no cells (background control), cells treated with medium (mock infection) and cells infected but untreated (infection control). After 20h, cells were incubated with Britelite plus reagent (Britelite plus kit; PerkinElmer) and then transferred to an opaque black plate. Luminescence was immediately recorded by a luminescence plate reader (LUMIstar Omega). To evaluate cytotoxicity, we used the CellTiter-Glo® Luminescent kit (Promega), following the manufacturer's instructions. Data was normalized to the mock-infected control, after which EC<sub>50</sub> and CC<sub>50</sub> values were calculated using Graph-Pad Prism 7.

## Modulation of ACE2 expression by anti-inflammatory drugs and immune stimuli

VeroE6 and lung cells were incubated with five-fold serial dilutions of selected anti-inflammatory compounds (ranging from 100µM to 0.8µM) for 20h. Tested drugs included cortisol, ibuprofen, prednisone and dexamethasone. Lung cells were also incubated with the following cytokines: GM-CSF (100 ng/ml, Immunotools), IL-1β (10 ng/ml, Immunotools), IL-10 (100 ng/ml, Immunotools), IFN-β (100 U/ml, Immunotools), or IFN-α2 (100 U/ml, Sigma Aldrich). For determination of ACE2 expression, the following surface staining antibodies were used: primary goat anti-ACE2 (R&D Systems), anti-CD45 (AF700, BioLegend), anti-EpCAM (APC, BioLegend), and anti-HLA-DR (BV421, BioLegend). For ACE2 detection, cells were then stained with secondary donkey anti-goat IgG (PE, R&D Systems) for 30 min at 4 °C. A Fluorescent Minus

One control (FMO) without primary anti-ACE2 antibody was used as a control. Cell viability was determined using an AQUA viability dye for flow cytometry (LIVE/DEAD fixable AQUA, Invitrogen). After fixation with PBS 2% PFA, cells were acquired in an LSR Fortessa (BD Biosciences) and analyzed using the FlowJo v10.6.1 software (TreeStar).

### **Immunomodulatory capacity of selected drugs**

HLT cells were cultured in a round-bottom 96-well plate containing 20  $\mu$ M of cepharanthine, ergoloid mesylate, ciclesonide, hydroxychloroquine, ivermectin, or camostat mesylate alone or in combination with the stimuli LPS (50 ng/ml) and IFN- $\gamma$  (100 ng/ml). For each patient, a negative control, cells treated with only medium, and a positive control, cells incubated in the presence of LPS and IFN- $\gamma$ , were included. Immediately, brefeldin A (BD Biosciences) and monensin (BD Biosciences) were added to cells and cultured overnight at 37 °C in 5% CO<sub>2</sub>. Next day, cellular suspensions were stained with the following antibodies: anti-CD11b (FITC, BioLegend), anti-CD69 (PE-CF594, BD Biosciences), anti-CD14 (APC-H7, BD Biosciences), anti-EpCAM (APC, BioLegend), anti-CD3 (BV650, BD Biosciences), anti-CD45 (BV605, BioLegend), and anti-HLA-DR (BV421, BioLegend). Cells were subsequently fixed and permeabilized using the Cytofix/Cytoperm™ kit (BD Biosciences) and intracellularly stained with anti-IL-6 (PE-Cy7, BioLegend), and anti-CXCL10 (PE, BioLegend). Cell viability was determined using an AQUA viability dye for flow cytometry (LIVE/DEAD fixable AQUA, Invitrogen). After fixation with PBS 2% PFA, cells were acquired in an LSR Fortessa (BD Biosciences), and data were analyzed using the FlowJo v10.6.1 software (TreeStar).

### **Statistical analyses**

Statistical analyses were performed with Prism software, version 6.0 (GraphPad). A P value <0.05 was considered significant.

### **Author contributions**

Conceptualization, M.J.B. and M.G.; Sample Collection, J.R.; Methodology J.G-E, D.P, M.S, N. M, A.V, M.J.S, J.G-P, J.A, A.S.M and V.F; Formal Analysis, J.G-E., D.P, M.S, M.G and M.J.B; Writing- Original Draft J.G-E and M.J.B; Writing- Review & Editing, J.G-E, M.G. and M.J.B; Funding Acquisition, M.G and M.J.B.; all authors revised the manuscript; Supervision, M.G and M.J.B.

### **Acknowledgments**

This work was primarily supported by a grant from the Health Department of the Government of Catalonia (DGRIS 1\_5). This work was additionally supported in part by the Spanish Health Institute Carlos III (ISCIII, PI17/01470), the Spanish Secretariat of Science and Innovation and FEDER funds (grant RTI2018-101082-B-I00 [MINECO/FEDER]), the Spanish AIDS network Red Temática Cooperativa de Investigación en SIDA (RD16/0025/0007), the European Regional Development Fund (ERDF), the Fundació La Marató TV3 (grants 201805-10FMTV3 and 201814-10FMTV3), the Gilead fellowships GLD19/00084 and GLD18/00008 and the Becas Taller Argal 2020. M.J.B is supported by the Miguel Servet program funded by the Spanish Health Institute Carlos III (CP17/00179). N.M. is supported by a Ph.D. fellowship from the Vall d'Hebron Institut de Recerca (VHIR). The funders had no role in study design, data collection and analysis, the decision to publish, or preparation of the manuscript.

# 539      **References**

- 540      1.      Beigel, J.H., et al., *Remdesivir for the Treatment of Covid-19 - Final Report*. N Engl J Med, 2020. **383**(19): p. 1813-1826.
- 541      2.      Consortium, W.H.O.S.T., et al., *Repurposed Antiviral Drugs for Covid-19 - Interim WHO Solidarity Trial Results*. N Engl J Med, 2021. **384**(6): p. 497-511.
- 542      3.      White, K.M., et al., *Plitidepsin has potent preclinical efficacy against SARS-CoV-2 by targeting the host protein eEF1A*. Science, 2021. **371**(6532): p. 926-931.
- 543      4.      Group, R.C., et al., *Dexamethasone in Hospitalized Patients with Covid-19*. N Engl J Med, 2021. **384**(8): p. 693-704.
- 544      5.      Takayama, K., *In Vitro and Animal Models for SARS-CoV-2 research*. Trends Pharmacol Sci, 2020. **41**(8): p. 513-517.
- 545      6.      Mossel, E.C., et al., *Exogenous ACE2 expression allows refractory cell lines to support severe acute respiratory syndrome coronavirus replication*. J Virol, 2005. **79**(6): p. 3846-50.
- 546      7.      Ortiz, M.E., et al., *Heterogeneous expression of the SARS-Coronavirus-2 receptor ACE2 in the human respiratory tract*. EBioMedicine, 2020. **60**: p. 102976.
- 547      8.      Hou, Y.J., et al., *SARS-CoV-2 Reverse Genetics Reveals a Variable Infection Gradient in the Respiratory Tract*. Cell, 2020. **182**(2): p. 429-446 e14.
- 548      9.      Koch, J., et al., *Host Cell Proteases Drive Early or Late SARS-CoV-2 Penetration*. bioRxiv, 2020.
- 549      10.      Hoffmann, M., et al., *SARS-CoV-2 Cell Entry Depends on ACE2 and TMPRSS2 and Is Blocked by a Clinically Proven Protease Inhibitor*. Cell, 2020. **181**(2): p. 271-280 e8.
- 550      11.      Ziegler, C.G.K., et al., *SARS-CoV-2 Receptor ACE2 Is an Interferon-Stimulated Gene in Human Airway Epithelial Cells and Is Detected in Specific Cell Subsets across Tissues*. Cell, 2020. **181**(5): p. 1016-1035 e19.
- 551      12.      Qiao, W., et al., *Ibuprofen attenuates cardiac fibrosis in streptozotocin-induced diabetic rats*. Cardiology, 2015. **131**(2): p. 97-106.
- 552      13.      Moore, N., et al., *Does Ibuprofen Worsen COVID-19?* Drug Saf, 2020. **43**(7): p. 611-614.
- 553      14.      Kutti Sridharan, G., et al., *COVID-19 and Avoiding Ibuprofen. How Good Is the Evidence?* Am J Ther, 2020. **27**(4): p. e400-e402.
- 554      15.      Xiang, Z., et al., *Glucocorticoids improve severe or critical COVID-19 by activating ACE2 and reducing IL-6 levels*. Int J Biol Sci, 2020. **16**(13): p. 2382-2391.
- 555      16.      Ravindra, N.G., et al., *Single-cell longitudinal analysis of SARS-CoV-2 infection in human bronchial epithelial cells*. bioRxiv, 2020.
- 556      17.      Si, L., et al., *Human organs-on-chips as tools for repurposing approved drugs as potential influenza and COVID19 therapeutics in viral pandemics*. bioRxiv, 2020: p. 2020.04.13.039917.
- 557      18.      Blanco-Melo, D., et al., *Imbalanced Host Response to SARS-CoV-2 Drives Development of COVID-19*. Cell, 2020. **181**(5): p. 1036-1045 e9.
- 558      19.      Lamers, M.M., et al., *An organoid-derived bronchioalveolar model for SARS-CoV-2 infection of human alveolar type II-like cells*. EMBO J, 2021. **40**(5): p. e105912.
- 559      20.      Kim, J., B.K. Koo, and J.A. Knoblich, *Human organoids: model systems for human biology and medicine*. Nat Rev Mol Cell Biol, 2020. **21**(10): p. 571-584.
- 560      21.      Chang, Y., et al., *Upregulation of IL-17A/F from human lung tissue explants with cigarette smoke exposure: implications for COPD*. Respir Res, 2014. **15**: p. 145.
- 561      22.      Hackett, T.L., et al., *Oxidative modification of albumin in the parenchymal lung tissue of current smokers with chronic obstructive pulmonary disease*. Respir Res, 2010. **11**: p. 180.
- 562      23.      Rimington, T.L., et al., *Defining the inflammatory signature of human lung explant tissue in the presence and absence of glucocorticoid*. F1000Res, 2017. **6**: p. 460.

- 589 24. Schaller, M.A., et al., *In vitro* infection of human lung tissue with SARS-CoV-2: Heterogeneity in host defense and therapeutic response. *bioRxiv*, 2021: p. 590 2021.01.20.427541.
- 592 25. Hasegawa, K., et al., Fraction of MHCII and EpCAM expression characterizes distal lung 593 epithelial cells for alveolar type 2 cell isolation. *Respir Res*, 2017. **18**(1): p. 150.
- 594 26. Singer, B.D., et al., Flow-cytometric method for simultaneous analysis of mouse lung 595 epithelial, endothelial, and hematopoietic lineage cells. *Am J Physiol Lung Cell Mol* 596 *Physiol*, 2016. **310**(9): p. L796-801.
- 597 27. Baharom, F., et al., Human Lung Mononuclear Phagocytes in Health and Disease. *Front* 598 *Immunol*, 2017. **8**: p. 499.
- 599 28. Katsumiti, A., et al., Immortalisation of primary human alveolar epithelial lung cells using 600 a non-viral vector to study respiratory bioreactivity in vitro. *Sci Rep*, 2020. **10**(1): p. 601 20486.
- 602 29. Qi, F., et al., Single cell RNA sequencing of 13 human tissues identify cell types and 603 receptors of human coronaviruses. *Biochem Biophys Res Commun*, 2020. **526**(1): p. 135- 604 140.
- 605 30. Wang, K., et al., CD147-spike protein is a novel route for SARS-CoV-2 infection to host 606 cells. *Signal Transduct Target Ther*, 2020. **5**(1): p. 283.
- 607 31. Qiao, Y., et al., Targeting transcriptional regulation of SARS-CoV-2 entry factors ACE2 608 and TMPRSS2. *Proc Natl Acad Sci U S A*, 2020.
- 609 32. Condor Capcha, J.M., et al., Generation of SARS-CoV-2 Spike Pseudotyped Virus for Viral 610 Entry and Neutralization Assays: A 1-Week Protocol. *Front Cardiovasc Med*, 2020. **7**: p. 611 618651.
- 612 33. Fukushi, S., et al., Vesicular stomatitis virus pseudotyped with severe acute respiratory 613 syndrome coronavirus spike protein. *J Gen Virol*, 2005. **86**(Pt 8): p. 2269-2274.
- 614 34. Kuba, K., et al., A crucial role of angiotensin converting enzyme 2 (ACE2) in SARS 615 coronavirus-induced lung injury. *Nat Med*, 2005. **11**(8): p. 875-9.
- 616 35. Ou, X., et al., Characterization of spike glycoprotein of SARS-CoV-2 on virus entry and its 617 immune cross-reactivity with SARS-CoV. *Nat Commun*, 2020. **11**(1): p. 1620.
- 618 36. Smith, M.D. and J.C. Smith, Repurposing Therapeutics for COVID-19: Supercomputer- 619 Based Docking to the SARS-CoV-2 Viral Spike Protein and Viral Spike Protein-Human ACE2 620 Interface.
- 621 37. Suffness, M. and J. Pezzuto, *Methods in plant biochemistry: assays for bioactivity*. 622 Academic Press, London, 1990: p. 71-133.
- 623 38. Yao, X., et al., In Vitro Antiviral Activity and Projection of Optimized Dosing Design of 624 Hydroxychloroquine for the Treatment of Severe Acute Respiratory Syndrome 625 Coronavirus 2 (SARS-CoV-2). *Clinical Infectious Diseases*, 2020. **71**(15): p. 732-739.
- 626 39. Maisonnasse, P. and J. Guedj, Hydroxychloroquine use against SARS-CoV-2 infection in 627 non-human primates. 2020. **585**(7826): p. 584-587.
- 628 40. Alméciga-Díaz, C.J., et al., Virtual Screening of Potential Inhibitors for SARS-CoV-2 Main 629 Protease. 2020, Preprints.org.
- 630 41. Hoffmann, M., et al., Camostat mesylate inhibits SARS-CoV-2 activation by TMPRSS2- 631 related proteases and its metabolite GBPA exerts antiviral activity. *bioRxiv*, 2020.
- 632 42. Lehrer, S., Inhaled biguanides and mTOR inhibition for influenza and coronavirus 633 (Review). *World Acad Sci J*, 2020. **2**(3).
- 634 43. Islam, A., et al., The pharmacological and biological roles of eriodictyol. *Arch Pharm Res*, 635 2020. **43**(6): p. 582-592.
- 636 44. Su, S. and S. Jiang, A suspicious role of interferon in the pathogenesis of SARS-CoV-2 by 637 enhancing expression of ACE2. *Signal Transduct Target Ther*, 2020. **5**(1): p. 71.
- 638 45. Vabret, N., et al., Immunology of COVID-19: Current State of the Science. *Immunity*, 639 2020. **52**(6): p. 910-941.



- 640 46. Smart, L., et al., *A narrative review of the potential pharmacological influence and safety*  
641 *of ibuprofen on coronavirus disease 19 (COVID-19), ACE2, and the immune system: a*  
642 *dichotomy of expectation and reality.* Inflammopharmacology, 2020. **28**(5): p. 1141-  
643 1152.
- 644 47. Shang, J., et al., *Cell entry mechanisms of SARS-CoV-2.* Proc Natl Acad Sci U S A, 2020.  
645 **117**(21): p. 11727-11734.
- 646 48. Valyaeva, A.A., et al., *Expression of SARS-CoV-2 entry factors in lung epithelial stem cells*  
647 *and its potential implications for COVID-19.* Sci Rep, 2020. **10**(1): p. 17772.
- 648 49. Kaufer, A.M., et al., *Laboratory biosafety measures involving SARS-CoV-2 and the*  
649 *classification as a Risk Group 3 biological agent.* Pathology, 2020. **52**(7): p. 790-795.
- 650 50. Walls, A.C., et al., *Structure, Function, and Antigenicity of the SARS-CoV-2 Spike*  
651 *Glycoprotein.* Cell, 2020. **183**(6): p. 1735.
- 652 51. Ogando, N.S., et al., *SARS-coronavirus-2 replication in Vero E6 cells: replication kinetics,*  
653 *rapid adaptation and cytopathology.* J Gen Virol, 2020. **101**(9): p. 925-940.
- 654 52. Lukassen, S., et al., *SARS-CoV-2 receptor ACE2 and TMPRSS2 are primarily expressed in*  
655 *bronchial transient secretory cells.* EMBO J, 2020. **39**(10): p. e105114.
- 656 53. Hamming, I., et al., *Tissue distribution of ACE2 protein, the functional receptor for SARS*  
657 *coronavirus. A first step in understanding SARS pathogenesis.* J Pathol, 2004. **203**(2): p.  
658 631-7.
- 659 54. Jeon, S., et al., *Identification of Antiviral Drug Candidates against SARS-CoV-2 from FDA-*  
660 *Approved Drugs.* Antimicrob Agents Chemother, 2020. **64**(7).
- 661 55. Rogosnitzky, M., P. Okediji, and I. Koman, *Cepharanthine: a review of the antiviral*  
662 *potential of a Japanese-approved alopecia drug in COVID-19.* Pharmacol Rep, 2020.  
663 **72**(6): p. 1509-1516.
- 664 56. Hoffmann, M., et al., *Chloroquine does not inhibit infection of human lung cells with*  
665 *SARS-CoV-2.* Nature, 2020. **585**(7826): p. 588-590.
- 666 57. Omrani, A.S., et al., *Randomized double-blinded placebo-controlled trial of*  
667 *hydroxychloroquine with or without azithromycin for virologic cure of non-severe Covid-*  
668 *19.* EclinicalMedicine, 2020. **29**: p. 100645.
- 669 58. Boulware, D.R., et al., *A Randomized Trial of Hydroxychloroquine as Postexposure*  
670 *Prophylaxis for Covid-19.* N Engl J Med, 2020. **383**(6): p. 517-525.
- 671 59. Mitja, O., et al., *Hydroxychloroquine for Early Treatment of Adults with Mild Covid-19: A*  
672 *Randomized-Controlled Trial.* Clin Infect Dis, 2020.
- 673 60. Ou, T., et al., *Hydroxychloroquine-mediated inhibition of SARS-CoV-2 entry is attenuated*  
674 *by TMPRSS2.* PLoS Pathog, 2021. **17**(1): p. e1009212.
- 675 61. Bray, M., et al., *Ivermectin and COVID-19: A report in Antiviral Research, widespread*  
676 *interest, an FDA warning, two letters to the editor and the authors' responses.* Antiviral  
677 Res, 2020. **178**: p. 104805.
- 678 62. Chaccour, C., et al., *The effect of early treatment with ivermectin on viral load, symptoms*  
679 *and humoral response in patients with non-severe COVID-19: A pilot, double-blind,*  
680 *placebo-controlled, randomized clinical trial.* EclinicalMedicine, 2021. **32**: p. 100720.
- 681 63. Onabajo, O.O., et al., *Interferons and viruses induce a novel truncated ACE2 isoform and*  
682 *not the full-length SARS-CoV-2 receptor.* Nat Genet, 2020. **52**(12): p. 1283-1293.
- 683 64. Ng, K.W., et al., *Tissue-specific and interferon-inducible expression of nonfunctional*  
684 *ACE2 through endogenous retroelement co-option.* Nat Genet, 2020. **52**(12): p. 1294-  
685 1302.
- 686 65. Busnadiego, I., et al., *Antiviral Activity of Type I, II, and III Interferons Counterbalances*  
687 *ACE2 Inducibility and Restricts SARS-CoV-2.* mBio, 2020. **11**(5).
- 688 66. de Lang, A., A.D. Osterhaus, and B.L. Haagmans, *Interferon-gamma and interleukin-4*  
689 *downregulate expression of the SARS coronavirus receptor ACE2 in Vero E6 cells.*  
690 *Virology*, 2006. **353**(2): p. 474-81.



67. Russell, A.B., C. Trapnell, and J.D. Bloom, *Extreme heterogeneity of influenza virus infection in single cells*. Elife, 2018. **7**.
68. Hall, K.C. and C.P. Blobel, *Interleukin-1 stimulates ADAM17 through a mechanism independent of its cytoplasmic domain or phosphorylation at threonine 735*. PLoS One, 2012. **7**(2): p. e31600.
69. Heurich, A., et al., *TMPRSS2 and ADAM17 cleave ACE2 differentially and only proteolysis by TMPRSS2 augments entry driven by the severe acute respiratory syndrome coronavirus spike protein*. J Virol, 2014. **88**(2): p. 1293-307.
70. Domingo, P., et al., *The four horsemen of a viral Apocalypse: The pathogenesis of SARS-CoV-2 infection (COVID-19)*. EBioMedicine, 2020. **58**: p. 102887.
71. Fraga-Silva, R.A., et al., *The angiotensin-converting enzyme 2/angiotensin-(1-7)/Mas receptor axis: a potential target for treating thrombotic diseases*. Thromb Haemost, 2012. **108**(6): p. 1089-96.
72. Cavalli, G., et al., *Interleukin-1 and interleukin-6 inhibition compared with standard management in patients with COVID-19 and hyperinflammation: a cohort study*. Lancet Rheumatol, 2021. **3**(4): p. e253-e261.
73. Liao, M., et al., *Single-cell landscape of bronchoalveolar immune cells in patients with COVID-19*. Nat Med, 2020. **26**(6): p. 842-844.
74. Chen, J.S., et al., *Non-steroidal anti-inflammatory drugs dampen the cytokine and antibody response to SARS-CoV-2 infection*. J Virol, 2021.
75. Zhang, D., et al., *COVID-19 infection induces readily detectable morphological and inflammation-related phenotypic changes in peripheral blood monocytes, the severity of which correlate with patient outcome*. medRxiv, 2020.
76. Fahlberg, M.D., et al., *Cellular events of acute, resolving or progressive COVID-19 in SARS-CoV-2 infected non-human primates*. Nat Commun, 2020. **11**(1): p. 6078.
77. Aggarwal, N.R., L.S. King, and F.R. D'Alessio, *Diverse macrophage populations mediate acute lung inflammation and resolution*. Am J Physiol Lung Cell Mol Physiol, 2014. **306**(8): p. L709-25.
78. Yamaya, M., et al., *The serine protease inhibitor camostat inhibits influenza virus replication and cytokine production in primary cultures of human tracheal epithelial cells*. Pulm Pharmacol Ther, 2015. **33**: p. 66-74.
79. Zhang, X., et al., *Ivermectin inhibits LPS-induced production of inflammatory cytokines and improves LPS-induced survival in mice*. Inflamm Res, 2008. **57**(11): p. 524-9.
80. Whitt, M.A., *Generation of VSV pseudotypes using recombinant DeltaG-VSV for studies on virus entry, identification of entry inhibitors, and immune responses to vaccines*. J Virol Methods, 2010. **169**(2): p. 365-74.
81. Li, M., et al., *Human immunodeficiency virus type 1 env clones from acute and early subtype B infections for standardized assessments of vaccine-elicited neutralizing antibodies*. J Virol, 2005. **79**(16): p. 10108-25.

## Figure legends

**Figure 1. Phenotyping of human lung cells.** (A). *t*-distributed Stochastic Neighbor Embedding (t-SNE) representation displaying the major cell clusters present in the CD45<sup>+</sup> and CD45<sup>-</sup>EpCam<sup>+</sup> fractions of a representative human lung tissue. The vertical bars in the right panel show the frequency of each subset relative to live cells. All cell subsets were identified as shown in Figure S1A. mDCs, myeloid dendritic cells; AT-II, alveolar type 2. (B). Phosphatase alkaline positive AT-II cells (pink staining) were detected in a cytospin obtained from human lung tissue cells and observed at 10x. Lower panel shows a high magnification (40x) of the black square. Scale bars are 100  $\mu$ m and 10  $\mu$ m in top and bottom panels, respectively. (C). *t*-distributed Stochastic Neighbor Embedding (tSNE) representation for ACE2, CD147 and TMPRSS2 expression in CD45<sup>+</sup> and CD45<sup>-</sup>EpCam<sup>+</sup> fractions from a representative lung tissue. Right graphs show the percentage of expression of each entry factor in the different cell subpopulations, which were identified as in Figure 1A with some modifications for the identification of myeloid cells and neutrophils (From big cells: monocytes/macrophages, CD11c<sup>+</sup>HLA-DR<sup>+</sup> CD14<sup>+</sup>; Alveolar macrophages and mDCs, CD11c<sup>+</sup> HLA-DR<sup>+</sup> CD14<sup>-</sup>; Neutrophils, CD11c<sup>-</sup> HLA-DR<sup>-</sup> CD14<sup>-</sup> CD3<sup>-</sup>). (D). Images of ACE2 immunohistochemical staining in human lung tissue sections at 40x magnification, counterstained with haematoxylin (top) or without (bottom). Black arrows indicate staining of ACE2 in AT-II cells (upper panel). Mean $\pm$ SEM is shown for all graphs.

**Figure 2. Susceptibility of VeroE6 and the HLT model to SARS-CoV-2 viral entry.** VeroE6 and HLT cells were infected with two different viral constructs (GFP and Luciferase) expressing the spike protein upon viral entry; VSV\* $\Delta$ G(GFP)-Spike and VSV\* $\Delta$ G(Luc)-Spike. (A) Representative flow cytometry plots of VeroE6 cells infected with VSV\* $\Delta$ G(GFP)-Spike or the background form VSV\* $\Delta$ G(GFP)-empty (left panel); and luciferase activity (RLUs; relative light units) at 20h post-infection with the pseudotyped VSV\*G(Luc)-G, the VSV\* $\Delta$ G(Luc)-Spike or the background form VSV\* $\Delta$ G(Luc)-empty (right panel). (B) Percentage of viral entry after treatment with anti-ACE2 antibody (10 $\mu$ g/ml) in VeroE6 cells infected with the pseudotyped virus expressing the control G protein or the spike from SARS-CoV-2. (C) A flow cytometry plot showing ACE2 expression in GFP<sup>+</sup> VeroE6 cells. Right graph shows mean fluorescence intensity (MFI) of ACE2 in both infected and uninfected fractions, based on GFP expression. (D) Representative flow cytometry plots of HLT cells infected with the viral construct expressing the spike protein (VSV\* $\Delta$ G(GFP)-Spike) or the background form (VSV\* $\Delta$ G(GFP)-empty) (left panel); and luciferase activity (RLUs; relative light units) at 20h post-infection with the VSV\* $\Delta$ G(Luc)-Spike or the background form VSV\* $\Delta$ G(Luc)-empty (right panel). Infection was measured as the percentage of GFP or RLUs, respectively. (E) Susceptible HLT cells to viral entry (identified as GFP<sup>+</sup> cells) compatible with an

AT-II phenotype, determined by the co-expression of HLA-DR and EpCAM in the CD45<sup>+</sup>CD31<sup>-</sup> fraction of live cells. (F) Bar plots showing the percentage of viral entry inhibition un HLT cells in the presence of anti-ACE2 antibody (15µg/ml), camostat (100µM) or anti-CD147 antibody (25µg/ml) after cell challenge with VSV\*ΔG(Luc)-Spike (left graph) or VSV\*ΔG(GFP)-Spike (right graph). Mean±SEM is shown for all graphs. Data in panel 2C were analyzed by a Wilcoxon matched-pairs test; \*p<0,05.

**Figure 3. Antiviral assays with concordant results between models.** (A). Percentage of viral entry in VeroE6 and HLT cells exposed to VSV\*ΔG(Luc)-Spike in the presence of cepharanthine, ergoloid, hydroxychloroquine, hypericin, licofelone, ivermectin, ciclesonide, quercetin, vidarabine and celecoxib. Drugs were used at concentrations ranging from 100µM to 0.256nM, in VeroE6, and to 0.8µM in lung cells. Non-linear fit model with variable response curve from at least two independent experiments in replicates is shown (red lines). Cytotoxic effect on VeroE6 cells and HLT exposed to drug concentrations in the absence of virus is also shown (green lines). (B). EC<sub>50</sub> values of each drug in VeroE6 and HLT cells. (C). CC<sub>50</sub> values of each drug are shown for VeroE6 and for HLT cells. (D). EC<sub>50</sub>'s coefficient of variation was calculated for ergoloid, hydroxychloroquine and cepharanthine in the HLT model. Data includes two independent experiments using different donors in replicates.

**Figure 4. Antiviral assays with discordant results between models.** (A). Percentage of viral entry in VeroE6 and HLT cells exposed to VSV\*ΔG(Luc)-Spike in the presence of luteolin, eriodictyol, phenformin, camostat, sulindac, and valaciclovir. Drugs were used at concentrations ranging from 100µM to 0.256 nM, in VeroE6, and to 0.8µM in lung cells. Non-linear fit model with variable response curve from at least two independent experiments in replicates is shown (red lines). Cytotoxic effect on VeroE6 cells and HLT exposed to drug concentrations in the absence of virus is also shown (green lines). (B). EC<sub>50</sub> values of each drug in VeroE6 and HLT cells. (C). CC<sub>50</sub> values of each drug are shown for VeroE6 and HLT cells.

**Figure 5. Impact of inflammation and anti-inflammatory drugs on SARS-CoV-2 viral entry and ACE2 expression.** Both models, HLT cells and VeroE6 cells, were incubated in the presence of different anti-inflammatory drugs to evaluate the modulation of ACE2 expression by flow cytometry and the antiviral effect by luminescence. (A). HLT cells were treated with different stimuli for 20h and the percentage of protein expression (left) or the mean fluorescence intensity (MFI, right) of ACE2 receptor was evaluated in the AT-II fraction by flow cytometry. (B) Modulation of ACE2 protein expression was assessed by flow cytometry in both models, Vero E6 and HLT cells, in the presence of different concentrations of each anti-inflammatory drug,

ranging from 100 $\mu$ M to 0.8 $\mu$ M. Percentage of ACE2 expression was quantified in AT-II cells from at least six independent lung samples, and in VeroE6 cells from 2 independent experiments. (C). Cytotoxic effect on Vero E6 and HLT cells exposed to VSV\* $\Delta$ G(Luc)-Spike in the presence of different concentrations of the anti-inflammatory drugs prednisone, cortisol, ibuprofen and dexamethasone. Drugs were used at a concentration ranging from 100 $\mu$ M to 0.256 nM, in VeroE6, and to 0.8 $\mu$ M in lung cells. Non-linear fit with variable response curve from at least two experiments in replicates is shown (red lines). Cytotoxic effect on Vero E6 cells and HLT cells exposed to different concentrations of drugs in the absence of virus is also shown (green lines). Mean $\pm$ SEM are shown and statistical comparisons with the control medium were performed using the Wilcoxon test. \* $p$ <0.05.

**Figure 6. Anti-inflammatory effect of compounds with antiviral activity against SARS-CoV-2.** HLT cells were cultured in the presence of 20 $\mu$ M of cepharanthine, ergoloid mesylate, ciclesonide, hydroxychloroquine sulfate, ivermectin or camostat mesylate, alone or in combination with the stimuli LPS (50 ng/ml) and IFN- $\gamma$  (100 ng/ml). (A) *t*-distributed Stochastic Neighbor Embedding (t-SNE) representations displaying the major cell clusters present in live CD45<sup>+</sup> myeloid gate, based on FSC and SSC, of a representative human lung tissue in baseline conditions and after stimulation with LPS and IFN- $\gamma$ . Two major subsets of myeloid cells are shown (CD11b<sup>+</sup> CD14<sup>+</sup>, in blue-green, and CD11b<sup>+</sup> CD14<sup>-</sup>, in orange). The expression of CXCL10 and IL-6 among the different populations is shown in maroon and green, respectively. (B) Expression of CXCL10 and IL-6 was measured in HLT cells in response to stimuli in the presence of selected drugs in both myeloid subpopulations, CD11b<sup>+</sup> CD14<sup>+</sup> (left panel) and CD11b<sup>+</sup> CD14<sup>-</sup> (right panel). HQ, hydroxychloroquine. Mean $\pm$ SEM are represented and statistical comparisons with the control medium were performed using the One sample t test. \* $p$ <0.05, \*\* $p$ <0.01.

**Figure S1. Gating strategy for the identification of cell subpopulations in the human lung tissue model.** (A) General gating strategy used to identify different cell subsets in lung samples. A gate based on FSC vs. SSC was followed by doublet and dead cells exclusion. From live CD45<sup>+</sup> cells, endothelial cells (CD31<sup>+</sup>, purple) and epithelial cells (EpCAM<sup>+</sup>, grey) were gated, and within epithelial cells, AT-II cells (EpCAM<sup>+</sup> and HLA-DR<sup>+</sup>, pink) were identified. Out of live CD45<sup>+</sup> cells and based on FSC vs. SSC, we identified a lymphocyte population in which we distinguished between non-T lymphocytes (turquoise) and T cells (dark green) based on CD3 expression; and big cells, where we identified three major subsets based on their expression of CD11b and CD11c and, subsequently, CD14 and HLA-DR markers. We identified alveolar macrophages (blue), monocytes (violet), myeloid dendritic cells (mDCs, fuchsia) and neutrophils (orange). (B)

830 Representative flow cytometry plots showing ACE2 staining and its respective fluorescence  
831 minus one (FMO) control.

832 **Figure S2. Optimization of lung tissue enzymatic digestion visualized by t-distributed**  
833 **Stochastic Neighbor Embedding (tSNE).** (A) Representative tSNE maps showing concatenated  
834 flow cytometry standard files for three different protocols based on different digestion enzymes  
835 (collagenase, liberase or trypsin) from total live cells (upper), CD45<sup>+</sup> cells (middle) and CD45<sup>-</sup> cells  
836 (lower). (B) Bar plots showing cell-type composition (count) analyzed by flow cytometry for each  
837 tissue protocol.

838 **Figure S3. Gating strategy for the identification of anti-inflammatory effects of selected**  
839 **compounds.** (A) General gating strategy used to evaluate the expression of inflammatory  
840 molecules in lung samples. A gate based on FSC vs. SSC was followed by doublet and dead cells  
841 exclusion. From live CD45<sup>+</sup> cells and based on FSC vs. SSC, we identified lymphocyte population  
842 and big cells, in which we identified two subsets based on their expression of CD11b and CD14:  
843 myeloid CD11b<sup>+</sup>CD14<sup>+</sup> cells (blue-green) and myeloid CD11b<sup>+</sup>CD14<sup>-</sup> cells (orange) are shown.



Figure 1

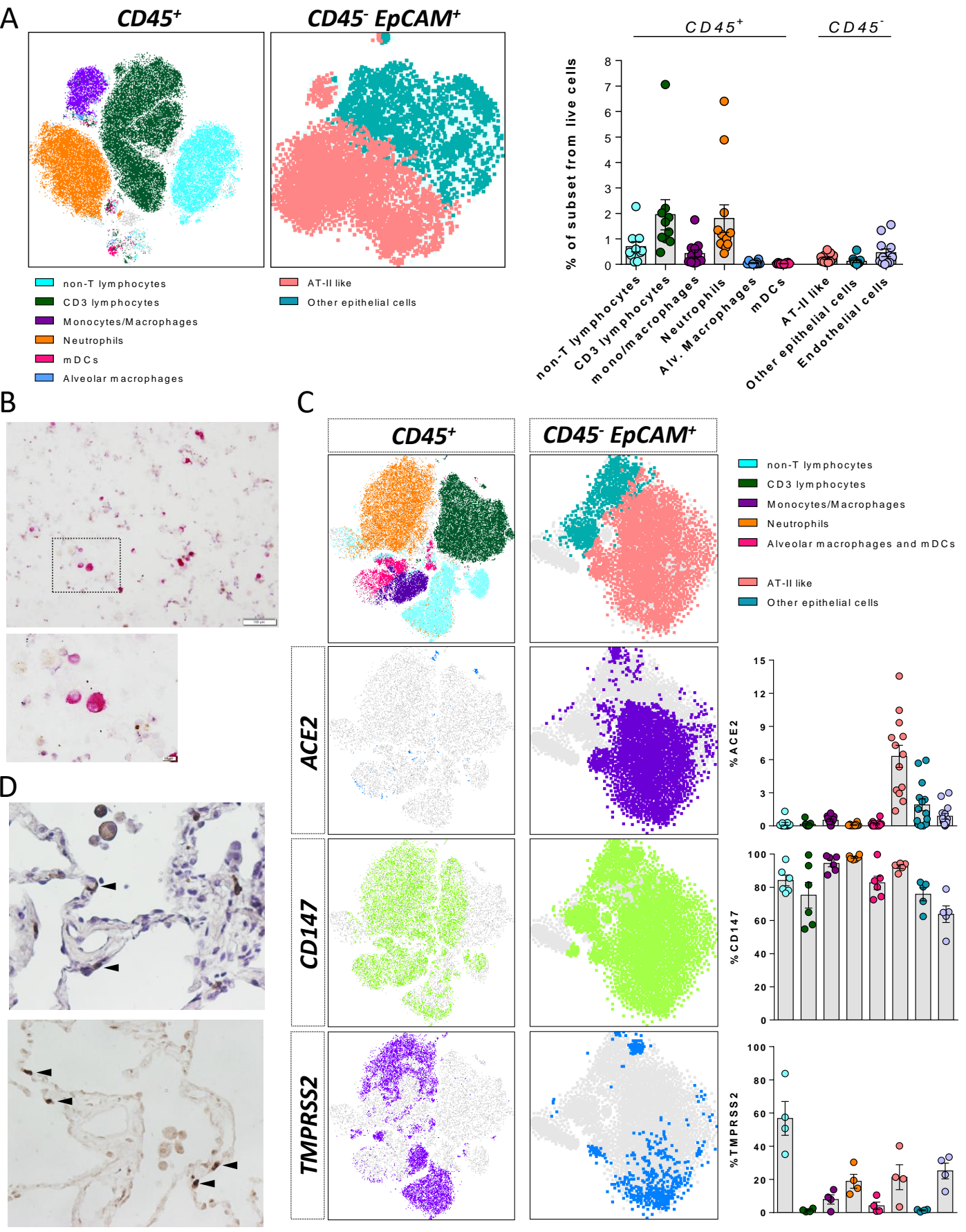


Figure 2

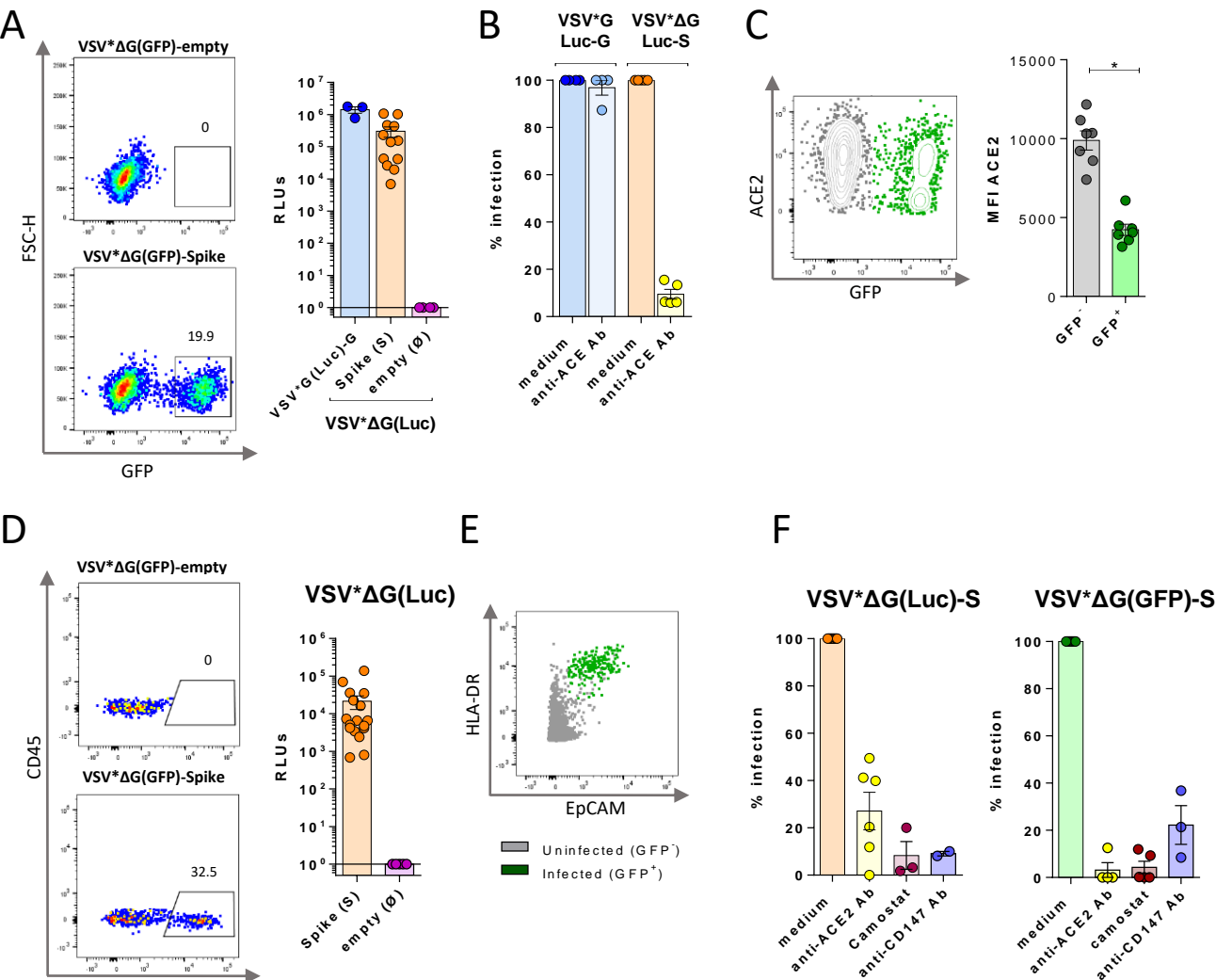
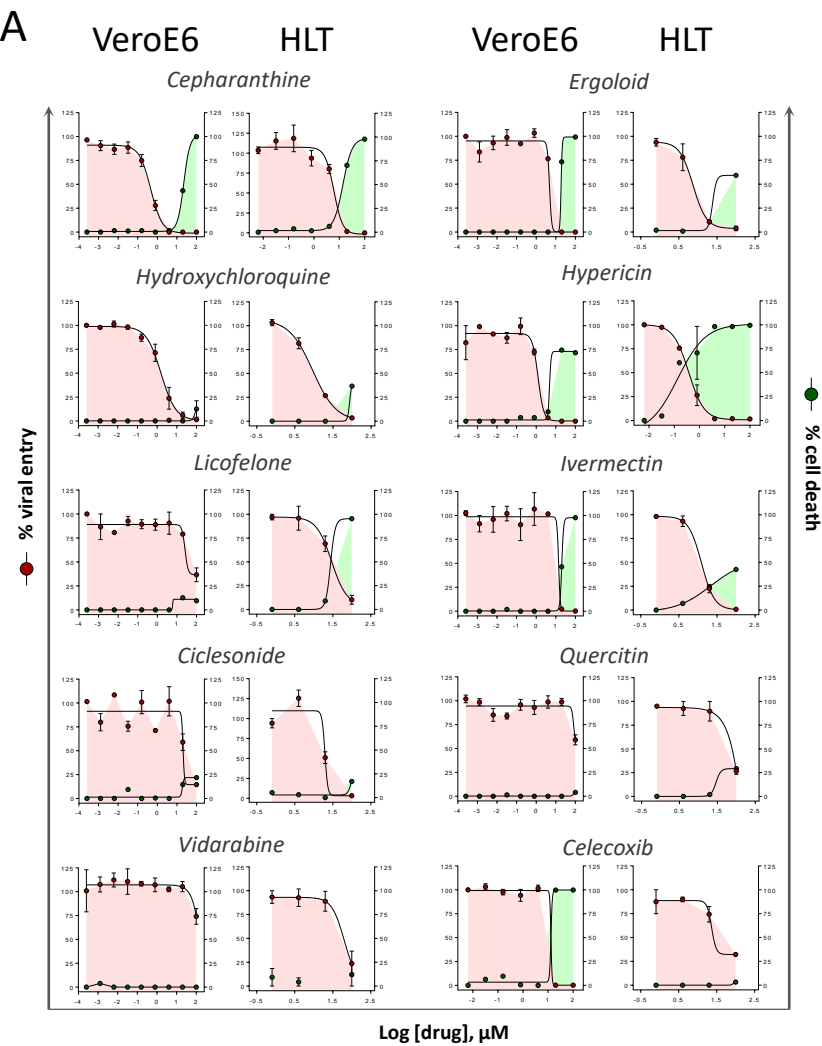




Figure 3



**B**

	VeroE6	HLT
Drugs	$\text{EC}_{50}$ ( $\mu\text{M}$ )	
Cepharanthine	0.4	6.1
Quercitin	>100	78
Ergoloid	4.7	7.7
Ciclesonide	20.5	19.6
Licofelone	87.5	29.3
Hydroxychloroquine	1.58	9.2
Ivermectin	13.9	12.4
Hypericin	1.2	0.37
Vidarabine	>100	66
Celecoxib	13	~25

**C**

	VeroE6	HLT
Drugs	$\text{CC}_{50}$ ( $\mu\text{M}$ )	
Cepharanthine	22.3	13.8
Quercitin	>100	>100
Ergoloid	18.6	~87.7
Ciclesonide	>100	>100
Licofelone	>100	29.4
Hydroxychloroquine	>100	>100
Ivermectin	20.23	>100
Hypericin	4.8	0.13
Vidarabine	>100	>100
Celecoxib	13	>100

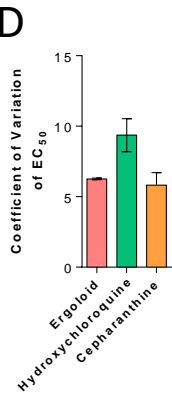
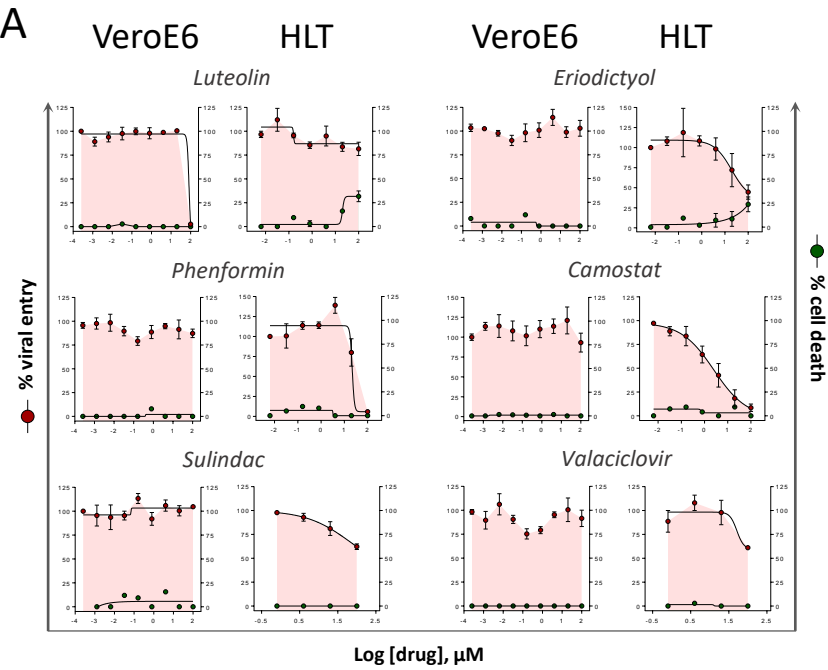


Figure 4



**B**

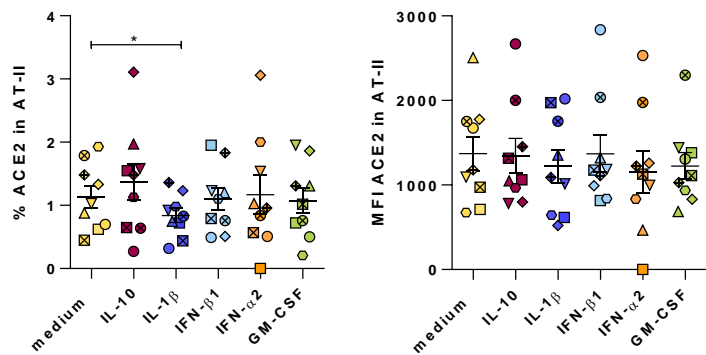
	VeroE6	HLT
Drugs	EC <sub>50</sub> ( $\mu\text{M}$ )	
Eriodictyol	no effect	90
Luteolin	~70.7	no effect
Camostat	no effect	2.7
Phenformin	no effect	~22.45
Sulindac	no effect	>100
Valaciclovir	no effect	>100

**C**

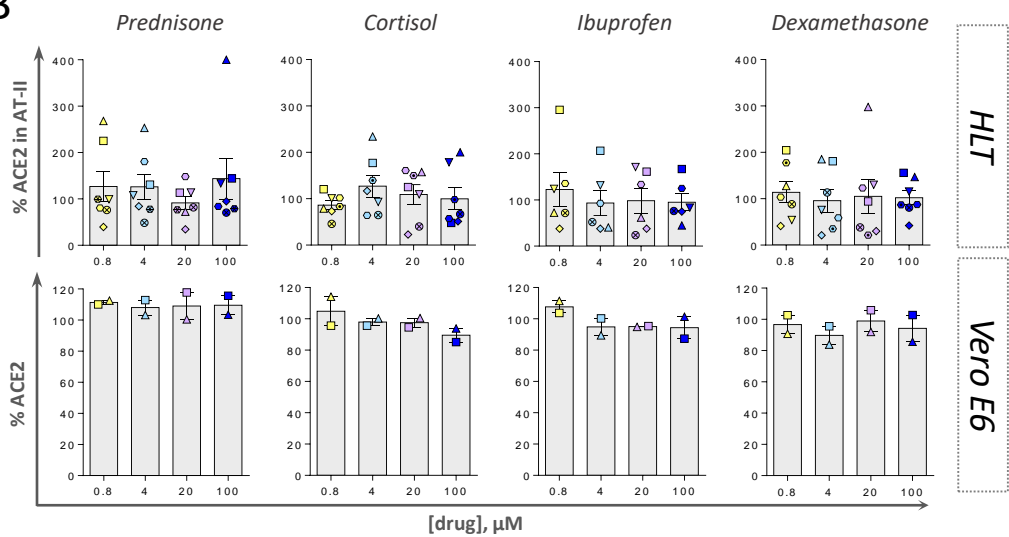
	VeroE6	HLT
Drugs	CC <sub>50</sub> ( $\mu\text{M}$ )	
Eriodictyol	>100	>100
Luteolin	>100	>100
Camostat	>100	>100
Phenformin	>100	>100
Sulindac	>100	>100
Valaciclovir	>100	>100

Figure 5

A



B



C

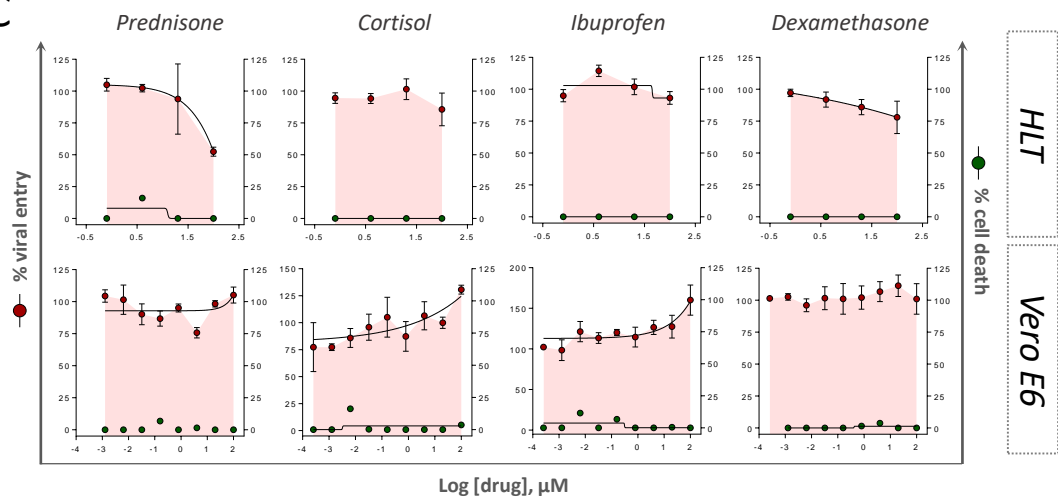


Figure 6

